Available online at www.sciencedirect.com

ScienceDirect

Ceramics International 40 (2014) 12509–12517

CERAMICS INTERNATIONAL

www.elsevier.com/locate/ceramint

Comparison of different fluorapatite dip coated layers on porous zirconia tapes

María P. Albano[a,1], Liliana B. Garrido[a], Lucas Novaes Teixeira[b], Adalberto Luiz Rosa[b], Paulo Tambasco de Oliveira[b]

[a]*Centro de Tecnología de Recursos Minerales y Cerámica (CETMIC), C.C. 49 (B1897ZCA) M.B. Gonnet, Provincia de Buenos Aires, Argentina*
[b]*Universidad de Sao Paulo-Facultad de Odontología de Ribeirao Preto (FORP-USP), Av. Do Café, s/n – Campus USP Monte Alegre, 14040-904 Ribeirao Preto, Sao Paulo, Brasil*

Received 20 March 2014; received in revised form 27 March 2014; accepted 28 March 2014
Available online 4 April 2014

Abstract

Fluorapatite (FA) layers with different thickness and microstructures on porous 3 mol% yttria-partially stabilized zirconia (Y-PSZ) substrates have been fabricated by dipping porous zirconia tapes into aqueous fluorapatite slurries. Porous ZrO_2 tapes were developed using starch and an acrylic latex as fugitive additive and binder, respectively. Two different binders, poly(vinyl)alcohol (PVA) and latex were used to prepare the fluorapatite dip coating slips. The influence of the suspension properties and the porous structure of the tape surfaces (top and bottom) on the formation rate and consequently on the layer thickness formed on each surface were studied. In addition, the microstructure of the layers produced by using the different dip-coating slips were compared and the osteoblastic cellular response to the different FA coating layers was examined. A greater initial thickness of the layer adhered was found for the tapes dip coated in the FA slip with latex; for immersion times > 0, the casting rate was observed to be strongly influenced by both the structure of the tape surfaces and the suspension properties. For both FA slurries, the casting rate at the top surface of the tapes was greater than that at the bottom surface. Sintered layers with thickness 8–9 times greater on both tape surfaces were found using the dip coating slip with latex. For each tape surface, the casting rate was accelerated and the layer shrink during sintering was reduced by using the dip coating slip with latex. The coating layer produced with latex enhanced the osteogenic potential of osteoblastic cells in vitro, which is ultimately an indication of the material's capacity to promote bone repair in vivo.

Keywords: Porous ZrO_2 tapesio; Fluorapatite layers; Dip coating; Osteoblastic cell response

1. Introduction

Calcium orthophosphates such as fluorapatite ($Ca_{10}(PO_4)_6F_2$) are widely used as bone substitute materials due to their chemical similarity to the mineral component of mammalian bones and teeth [1,2]. Fluorapatite is non-toxic, biocompatible, not recognized as foreign material in the body and, most importantly, exhibits bioactive behavior and integrates into living tissue by the same processes active in remodeling healthy bone. These characteristics lead to an intimate physicochemical bond between the implants and bone, termed osteointegration [3]. Even so, the major limitations to use fluorapatite as load-bearing biomaterials is its mechanical properties, it is brittle with a poor fatigue resistance [4]. The poor mechanical behavior is even more evident for highly porous ceramics and scaffolds [5]; that is why, in biomedical applications fluorapatite is used primarily as fillers and coatings. Bioinert ceramic such as porous ZrO_2 can be coated with FA to achieve a high mechanical strength as well as a suitable biocompatibility of the system [6,7].

The currently used coating methods, such as plasma spraying, sol–gel synthesis, physical vapor deposition and dip coating, have their own advantages as well as shortcomings. The coating layer by the plasma-spraying technique is thick ($\sim$50–200 μm) and relatively dense; however, phase instability and non-uniformity are some of its weaknesses [8]. The

E-mail address: palbano@cetmic.unlp.edu.ar (M.P. Albano).
[1]Fax: +54 221 471 0075.

http://dx.doi.org/10.1016/j.ceramint.2014.03.166
0272-8842/

films synthesized by sol–gel and physical vapor deposition methods are relatively uniform and the fabrication method is simple; however, the layer is too thin (~1 μm) to be applied for long-term usage [9,10]. Coating layers dense and uniform with thickness of 5–20 μm retaining high chemical and thermal stability can be produced by dip coating. When a dry porous substrate is dipped into a ceramic suspension and subsequently withdrawn from it, a wet dense cake of well-defined thickness can be formed on the substrate surface. After being dried and sintered, a ceramic layer is achieved.

We have previously studied the tape casting process to produce porous zirconia substrates using starch and an acrylic latex emulsion as fugitive additive and binder, respectively [11]. Besides, the processing of stable concentrated aqueous FA suspensions with the addition of ammonium polyacrylate (NH_4PA) and Poly(vinyl)alcohol (PVA) as dispersant and binder, respectively, was investigated [12]. In this work, porous Y-PSZ tapes with 31.4 vol% porosity were produced by tape casting and characterized with specific attention directed to the microstructure of the top and bottom surfaces of the sintered tapes. Then, sections of these tapes were dip coated into the different concentrated aqueous FA slurries to produce FA layers.

Two mechanisms govern the formation of a layer on a porous body during dip coating. The first mechanism is known as liquid entrainment, and occurs as the plate-like specimen is withdrawn from the slurry faster than the liquid can drain from its surface, leaving a thin slurry film [13]. The second mechanism is slip casting, the capillary suction caused by the porous substrate drives ceramic particles to concentrate at the substrate-suspension boundary, and a wet layer is formed [14]. The withdrawal velocity of the specimen and the suspension viscosity have influence on the liquid entrainment mechanism. The microstructure of the substrate (porosity and pore diameter) together with the structure of the wet layer have influence on the slip casting mechanism. In this work, two different binders PVA and an acrylic latex emulsion were used to prepare the FA suspensions. The influence of the suspension properties and the porous structure of the tape surfaces (top and bottom) on the formation rate and consequently on the layer thickness formed on each surface were studied. In addition, the microstructure of the layers produced by using the different dip coating slips were compared and the osteoblastic cell response to the different FA coating layers was assessed in terms of cell morphology, proliferation and matrix mineralization. These results would be essential to the fabrication of FA layers with different thickness and microstructures on porous zirconia tapes using the dip coating procedure.

2. Experimental procedure

2.1. Raw materials and processing

A commercial 3 mol% yttria-partially stabilized zirconia doped with 0.3 wt% Al_2O_3 (Saint-Gobain ZirPro, Chine) was used to produce the cast tapes. The mean particle diameter and the specific surface area were 0.15 μm and 12.25 m^2/g, respectively. Potato starch commercially available in Argentina was used as pore former agent. The starch granules exhibit a small degree of anisotropy with a median equivalent diameter of about 50 μm.

A commercial ammonium polyacrylate (NH_4PA) solution (Duramax D 3500, Rohm & Haas, Philadelphia, PA) was used as a dispersant. The binder was an acrylic latex emulsion (Duramax B1000, Rohm & Haas, Philadelphia PA) with solids loading of 55 wt%, an average particle size of 0.37 μm, and a glass transition temperature of −26 °C.

The $Ca_3(PO_4)_2$ (Fluka, Germany) and CaF_2 (Sigma-Aldrich, Ireland) powders were mixed in stoichiometric ratio and calcined 3 h at 1000 °C. Then, the powder was milled in an attrition mill using 1.6 mm zirconia balls with 0.047 wt% NH_4PA during 48 h. The milled powder was washed with distilled water and dried at 100 °C. This powder subsequently referred as FA was used to prepare the suspensions for dip coating. NH_4PA was used as deflocculant and two different binders a 9 wt% PVA solution and the acrylic latex emulsion were employed to prepare the different FA suspensions. The degree of hydrolysis of PVA was 87–89% and the average molecular weight was in the range of 57,000–66000 g/mol.

Concentrated aqueous Y-PSZ suspensions with a solid loading of 77 wt% were prepared by deagglomeration of the powder in distilled water with 0.3 wt% NH_4PA (dry weight base of powder) using an ultrasonic bath. 13 wt% of starch (dry weight base of Y-PSZ powder) was added to the stabilized Y-PSZ slips followed by ultrasonic treatment. Subsequent to this, 25 wt% latex (dry weight basis with respect to (Y-PSZ + starch) powders) was added to the slurry, followed by additional stirring. The pH of the suspensions was adjusted to 9.0 with ammonia (25 wt%).

The Y-PSZ slips were cast manually on a Mylar film using an extensor. The gap between the extensor and the film was adjusted to 0.4 mm. The cast tapes were subsequently dried in air at room temperature up to constant weight; afterwards, they were stripped from the film and sectioned into rectangular pieces of 2.75 cm × 1.65 cm. The burn out of organic additives was achieved by slow heating (1 °C/min) up to 1000 °C. Then, the pre-calcined tapes were sintered at 1500 °C for 2 h, with a heating rate of 5 °C/min.

Aqueous FA slips with 0.6 wt% NH_4PA and different contents of the two binders: 5 wt% PVA and 15 wt% latex, were prepared by suspending particles in deionized water via 20 min of ultrasound; the pH was manually adjusted to be maintained at 9. The sintered tapes were vertically dipped into the FA suspension; after immersion during different times they were withdrawn from the suspension. All specimens were immersed and withdrawn at a constant rate of 8 mm/s. The dip-coated samples were allowed to dry at room temperature in the vertical orientation, further dried in air at 60 °C, heated for 30 min at 600 °C for binder burn out and sintered at 1200 °C for 1h.

The biological assays was carried out using Y-PSZ discs, 12 mm in diameter and 3 mm thickness, produced by slip casting and sintered at 1500 °C for 2 h; the Y-PSZ discs had

nearly full density (> 98% theoretical density). The discs were then dipped into the different FA suspension for 120 s, dried and sintered as described for the coated tapes.

2.2. Characterization techniques

The microstructure of sintered samples were observed on both the top side of the tape (exposed to air during casting/drying), and the bottom side (exposed to the carrier surface during casting/drying) using a scanning electron microscopy (SEM) (JEOL, JSM-6360). The fractured surfaces of the tapes were also examined by SEM.

The viscosity of the aqueous FA slips with 0.6 wt% NH_4PA and different contents of the two binders: 5 wt% PVA and 15 wt% latex were measured. Steady state flow curves of FA slips were performed by measuring the steady shear stress value as a function of shear rate in the range of 0.5–542 s^{-1} using a concentric cylinder viscometer (Haake VT550, Germany) at 25 °C. A coaxial cylinder system with two gaps (sensor system NV Haake) was used. As soon as stationary conditions were reached at each shear rate, the shear rate increased in steps up to the maximum value and then decreased.

Dipped tapes were diamond polished and examined by SEM; the layer thickness on the top and bottom surfaces were measured. The microstructure of the FA coating layer after sintering produced using the different dip coating slips was observed by SEM.

2.3. Biological assays

2.3.1. Cell culture

The MC3T3-E1 cell lineage (subclone 14) was obtained from the American Type Culture Collection (ATCC) and cultured in Dulbecco's modified Eagle medium (DMEM; Gibco, Invitrogen, Grand Island, NY) supplemented with 10% fetal bovine serum (Gibco), 100 U/ml penicillin (Invitrogen) and 100 μg/ml streptomycin (Invitrogen) in 75 cm^2 flasks (Corning Incorporated, Costar, Corning, NY). The cultures were incubated at 37 °C in a humidified atmosphere of 5% CO_2 and 95% air. The medium was changed every 2 or 3 days. At confluence, cells were harvested after treatment with 1 mM ethylenediamine tetraacetic acid (EDTA) (Gibco) and 0.25% trypsin (Gibco). Then, the cells were plated on the discs in 24-well polystyrene culture plates (Corning) at a cell density of 2×10^4 cells/well and cultured for up to 21 days. The cells were grown in osteogenic medium containing DMEM (Gibco) supplemented with 10% fetal bovine serum (Gibco), 100 U/ml penicillin (Invitrogen), 100 μg/ml streptomycin (Invitrogen), 5 μg/mL ascorbic acid (Gibco), and 7 mM β-glycerophosphate (Sigma, St. Louis, MO). During the culture period, cells were incubated at 37 °C in a humidified atmosphere of 5% CO_2 and 95% air. The medium was changed every 2 or 3 days.

2.3.2. Cell morphology

At 3, 7 and 12 days, cell morphology was evaluated by direct fluorescence as described elsewhere [15]. Osteoblastic cells were fixed for 10 min at room temperature (RT) using 4% paraformaldehyde in 0.1 M sodium phosphate buffer (PB), pH 7.2. After being washed in PB, cultures were permeabilized with 0.5% Triton X-100 in PB for 10 min and processed for fluorescence labeling. Alexa fluor 488 (green fluorescence)-conjugated phalloidin (1:200, Molecular Probes, Eugene, OR) was used to label actin cytoskeleton. Before mounting for microscope observation, samples were briefly washed with deionized water (dH_20), and the cell nuclei were stained with 300 nM 40,6-diamidino-2-phenylindole, dihydrochloride (DAPI, Molecular Probes) for 5 min. The discs were placed face up on glass slides, covered with 12-mm round glass coverslips (Fisher Scientific) and mounted with an antifade kit (Vectashield, Vector Laboratories, Burlingame, CA). The samples were then examined under epifluorescence, using a Zeiss AxioImager M2 microscope (Carl Zeiss, Oberkochen, Germany) outfitted with a AxioCam MRm digital camera (Carl Zeiss). Acquired digital images were processed with Adobe Photoshop CS5.1 software (Adobe Systems).

2.3.3. Cell proliferation

Cell proliferation was evaluated by 3-[4,5-dimethylthiazol-2-yl]-2,5-diphenyl tetrazolium bromide (MTT, Sigma) assay [16]. At 3, 7 and 12 days, the osteoblastic cells were incubated with 10% of MTT (5 mg/ml) in culture medium at 37 °C for 4 h. The medium was then aspirated from the well, and 1 ml of acid isopropanol (0.04 N HCl in isopropanol) was added to each well. The plates were then stirred on a plate shaker for 5 min, and 150 μl of this solution was transferred to a 96-well format using opaque-walled transparent-bottomed plates (Corning). The optical density was read at 570–650 nm on the plate reader (μQuanti, BioTek Instruments, Inc., Winooski, VT, EUA), and data were expressed as absorbance.

2.3.4. Matrix mineralization

At day 21, cultures grown on the discs were fixed in 10% formalin for 2 h at RT, dehydrated and stained with 2% Alizarin Red S (Sigma), pH 4.2, for 10 min. The calcium content was detected using a colorimetric method [17]. Briefly, 280 μl of 10% acetic acid were added to each well and the plate was incubated at RT for 30 min under shaking. This solution was vortexed for 1 min, heated to 85 °C for 10 min, and transferred to ice for 5 min. The slurry was centrifuged at 13,000*g* for 15 min and 100 μl of the supernatant was mixed with 40 μl of 10% ammonium hydroxide. The optical density was read at 405 nm on the plate reader (μQuanti), and data were expressed as absorbance.

2.3.5. Statistical analysis

All data were expressed as means ± standard deviation. Statistical comparisons of the results were performed using the non-parametric Kruskal–Wallis test, followed by the Student–Newman–Keuls test. The level of significance was 5%.

3. Results and discussion

3.1. Fluorapatite surface coating

Two mechanisms govern the formation of a layer on a porous body during dip coating. The first mechanism is known as liquid entrainment, and ocurrs as the plate-like specimen is withdrawn from the slurry faster than the liquid can drain from its surface, leaving a thin slurry film [13]. This film thickness, h, is given by:

$$h = 0.94(\gamma/\delta g)^{1/2}\mathrm{Ca}^{2/3} \quad (1)$$

Ca is the capillary number given by [13]:

$$\mathrm{Ca} = \eta V/\gamma \quad (2)$$

where γ is the surface tension, δ is the slurry density, g is the gravity acceleration, η is the slurry viscosity and V is the withdrawal velocity. As the liquid from the thin layer of slurry evaporates, a thin coating of ceramic particles remains on the surface of the specimen. The second mechanism is a slip-casting phenomenon and occurs because the tapes, when dipped, are slightly porous and dry. The capillary suction caused by the porous substrate drives ceramic particles to concentrate at the substrate-suspension boundary, and a wet membrane, or cake, is formed, as in the slip casting process [14]. In this capillary filtration, the driving force is the capillary suction pressure caused by all the pores on the surface of the substrate. Fluid flow through the consolidated layer and into the porous body is governed by Darcy's law, which can be integrated and simplified (assuming that the permeability of the substrate is much larger than that of the layer) to express the thickness of the wet layer, L, as a function of time, t, in the form [14]:

$$L = 2(\varepsilon_s \gamma k_m t/\mu\, \alpha\, R)^{1/2} \quad (3)$$

where ε_s is the porosity of the substrate, k_m is the permeability of the wet layer, t is the time, R is the pores radius and μ represents the dispersion liquid viscosity; α is defined as:

$$\alpha = (\varphi_m/\varphi_0) - 1 \quad (4)$$

where φ_0 and φ_m are the volume fraction of the particles in the suspension and in the wet layer, respectively. During the subsequent drying and sintering process, the layer shrinks only in the direction perpendicular to the substrate, the thickness of the sintered layer, $L_{sintered}$, can be expressed as [14]:

$$L_{sintered} = \beta L \quad (5)$$

where β is defined as:

$$\beta = \varphi_m/(1-\varepsilon_m) \quad (6)$$

ε_m is the porosity of the sintered layer. Substituting Eqs. (3) and (6) into Eq. (5) gives:

$$L_{sintered} = [2\varphi_m/(1-\varepsilon_m)](\varepsilon_s \gamma k_m t/\mu\alpha R)^{1/2} \quad (7)$$

Fig. 1 shows the layer thickness after sintering versus immersion time for the top and bottom surfaces of the tapes dip coated in the different FA suspensions. The layer thickness squared versus immersion time for the tapes dip coated in the FA slurries prepared with PVA and latex are shown in Fig. 2a and b, respectively.

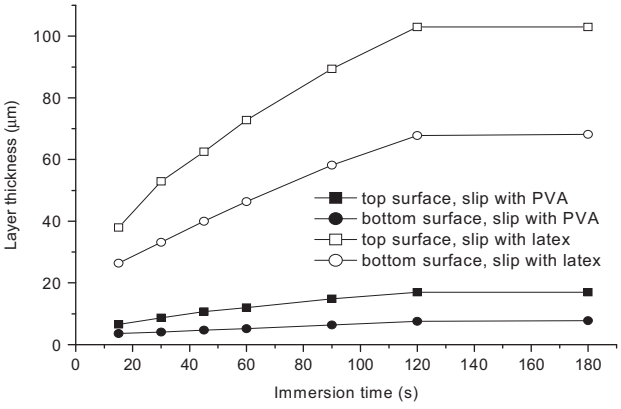

Fig. 1. Layer thickness after sintering versus immersion time for the top and bottom surfaces of the tapes dip coated in the different FA suspensions.

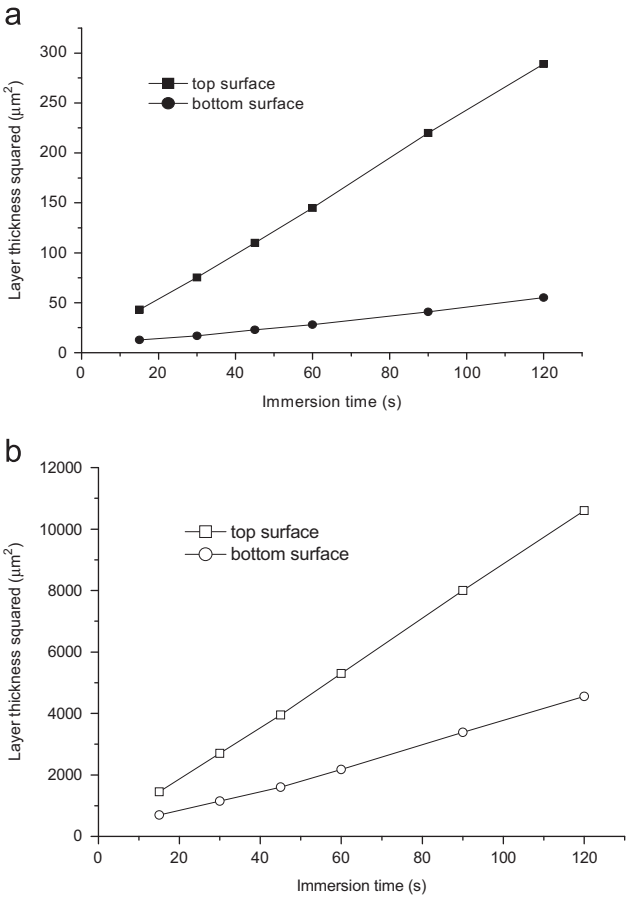

Fig. 2. Layer thickness squared after sintering versus immersion time for the tapes dip coated in the FA slurries prepared with the different binders: (a) PVA and (b) latex.

Fig. 3a and b shows the flow curves of shear stress versus shear rate and viscosity versus shear rate, respectively, at pH 9 for the different FA slips. The measured flow curves were satisfactorily fitted with the Casson model (R = 0.99). The

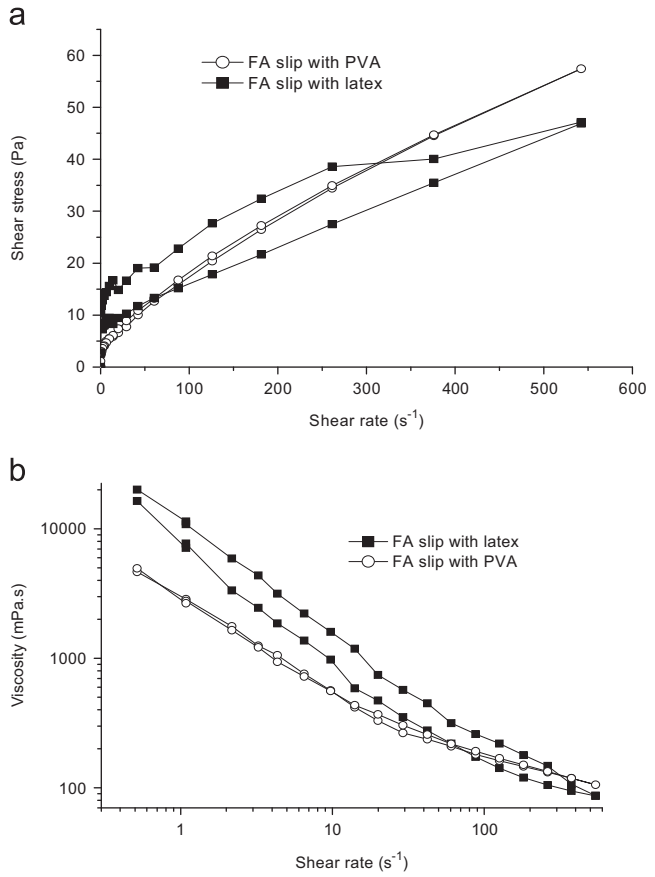

Fig. 3. (a) Flow curves of shear stress versus shear rate and (b) viscosity versus shear rate, at pH 9 for the different FA slips.

Casson model equation is:

$$\tau^{1/2} = \tau_0{}^{1/2} + (\eta_p \gamma)^{1/2} \quad (8)$$

where τ is the shear stress, γ is the shear rate, τ_0 is the yield stress and η_p represents the limiting viscosity at a high shear rate range. The particles in a flocculated suspension form floc groups or a network, because of the mutual attraction between particles, and the yield stress value of the Casson model could be used as a parameter that indicated the degree of aggregation and consequently the degree of slip flocculation. The η_p value becomes equal to the viscosity when $\tau_0 \rightarrow 0$. Table 1 shows the composition and rheological parameters of the different FA slips. The slips exhibited a pseudoplastic behavior; thus, the slip viscosity decreased with increasing the shear rate and the slips prepared with latex show a strong shear thinning tendency (Fig. 3a and b). In the regime of low shear rates as proceeds in the dip coating process [13], higher shear stress and viscosity values were found for the FA slips prepared with latex with respect to those for the slips with PVA. The low τ_0 value of the slip prepared with PVA indicated a weak flocculation; while the slip with latex was strongly flocculated with an attractive network (high τ_0 value, Table 1). The higher resistance to flow of the slip with latex avoided any settling of the particles by reducing their mobility. The high volume fraction of solids and τ_0 value of the slip with latex contributed to increase the slip viscosity.

Table 1
Composition and rheological parameters of the different FA slips.

FA slips	Volume fraction of solids (%)	τ_0 (Pa)	η_p (Pa s)
With PVA	27.4	1.86	0.076
With latex	36.2	7.62	0.052

The lines in Fig. 2a and b did not pass through the origin instead they intersected the *y*-vertical axis at a thickness value of about 13 and 3 μm for the slips prepared with latex and PVA, respectively. As we have previously mentioned the first mechanism in the layer formation was the liquid entrainment which leaves a thin slurry film on the tape surface (Eqs. (1) and (2)). As the viscosity values at low shear rates (0.5–1 s^{-1}) of the slips with latex were four times higher than those of the slips with PVA (Fig. 3b), a greater thickness of the film adhered, *h*, could be expected. Thus, the film thickness given by Eq. (1) was not dependent on the structures of the porous surface, instead it was dependent on the slurry viscosity. As the data for the different slips were obtained by using identical withdrawal velocity, the greater thickness of the layer produced using the slip with latex at the initial stage was attributed to the higher viscosity of the slip with latex and its effect on the liquid entrainment mechanism.

The Eq. (3) shows that when the suspension and substrate are fixed, the layer thickness squared increases linearly with the dipping time. The increase in the immersion time produced significantly thicker layers up to reaching saturation of the tapes at 120 s (Fig. 1). A linear relation between the thickness squared and the dipping time up to 120 s was found (Figs. 2a and b), suggesting that these data were in good agreement with the Eq. (3) for the casting mechanism. For immersion times > 0, the casting rate was observed to be strongly influenced by both the structure of the tape surfaces and the suspension properties (Figs. 1 and 2).

In a previous paper, the authors characterized the top and bottom surfaces of the tapes with a total bulk porosity of 31.4 vol% and an open porosity of 16 vol% [18]. Fig. 4 shows micrographs of the top and bottom surfaces of the sintered tape. As we have mentioned the top surface was exposed to air during casting/drying while the bottom one was in contact with the film carrier. The surfaces were different; a greater number of large pores created by the starch particles (lengths between 15 and 80 μm) (Fig. 4a and b) and also a greater number of smaller pores in the matrix (lengths between 0.6 and 3.0 μm) (Fig. 4c and d) were found on the top surface with respect to those on the bottom one. The starch particles migrated to the top surface during casting due to its lower density (1.45 g/cm^3) in comparison with 6.05 g/cm^3 for Y-PSZ. In addition, the latex particle clusters migrated in the same direction as the solvent, to the top surface, as drying proceeded [18]. Thus, the migration of the starch and the consolidated latex particles to the top surface during casting and drying, respectively, resulted in an increase in porosity of the top surface after sintering relative to that of the bottom surface. Some of the pores interacted and an open structure interconnecting the pores was

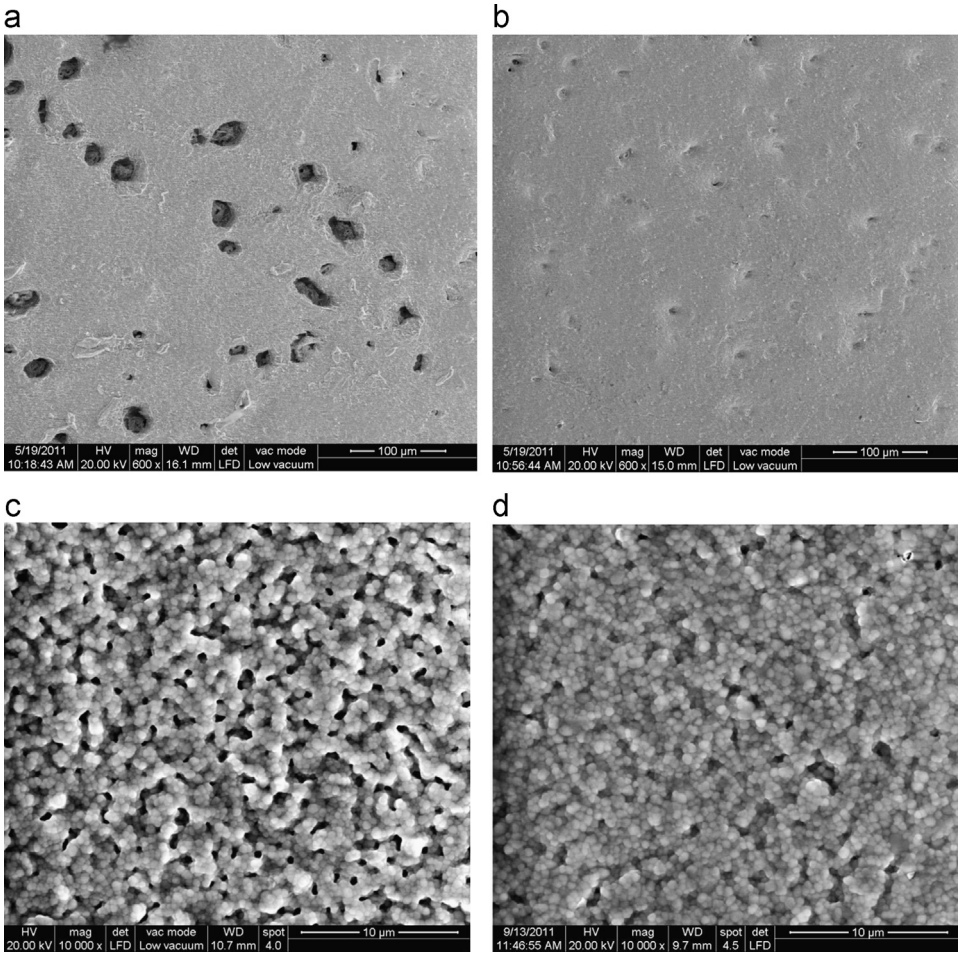

Fig. 4. SEM micrographs of the sintered tape surfaces: (a) top surface; (b) bottom surface; (c) top surface matrix; and (d) bottom surface matrix.

established. The interconnection open paths and channels between pores which finally result in open porosity [18]. The greater porosity and the larger number of smaller pores increased the casting rate (Eq. (3)) of the top surface producing thicker dip coated layers. Layers formed on the top surface were found to be about 50 % and 36% thicker than those formed on the bottom surface, for the tapes dip coated in the FA suspension with PVA and latex, respectively.

The FA slip prepared with latex produced significantly thicker layers on both tape surfaces relative to the slip prepared with PVA (Fig. 1). A comparison of the line slopes for each tape surface (Fig. 2) indicated that the casting rate of the slip with latex was greater with respect to that with PVA, resulting in an increase of the layer thickness. As it was mentioned, the layer formation process by dip coating is similar to the formation of a cake on a porous mould by slip casting [14] in both the driving force for the liquid flow is the capillary suction pressure of the substrate. We have previously studied the casting rate of FA suspensions with different viscosities and the microstructure of the resultant green slip cast cakes [19]. Our results demonstrated that the volume and size of the most frequent pore radius within the cake increased when a flocculated slip with high viscosity was cast. The greater porosity and pore size increased the permeability of the cake, thereby increasing the casting rate. In well dispersed slips with low viscosity values the particles could pack in an ordered and dense way due to the repulsive forces existing between them, resulting in a lower permeability of slip cast bodies [19]. In this work, a greater permeability of the wet layer produced with the FA slip prepared with latex (high τ_0 value) and consequently a greater casting rate could be expected. Thus, the higher casting rate of the slips with latex on both tape surfaces was attributed to the greater permeability of the wet layer (Eq. (3)). On the contrary for the slips with PVA, the increase in the dispersion liquid viscosity (μ) due to the water soluble PVA [20] together with the lower permeability of the wet later (low τ_0 value), both produced a decrease in the casting rate (Eq. (3)).

Fig. 5 shows the microstructure of the FA coating layer after sintering produced using the different dip coating slips. A greater porosity and pore size of the FA sintered layer was found when the dip coating slurry was prepared with latex. The FA sintered layer produced using the dip coating slurry with latex had rounded and elongated pores with lengths between 1.0 and 5.6 µm; while the layer formed using the slip with PVA had smaller pores with lengths between 0.4 and 3.1 µm. For the layer produced using the slip with latex, the coalescence of the latex particles during drying and the pore

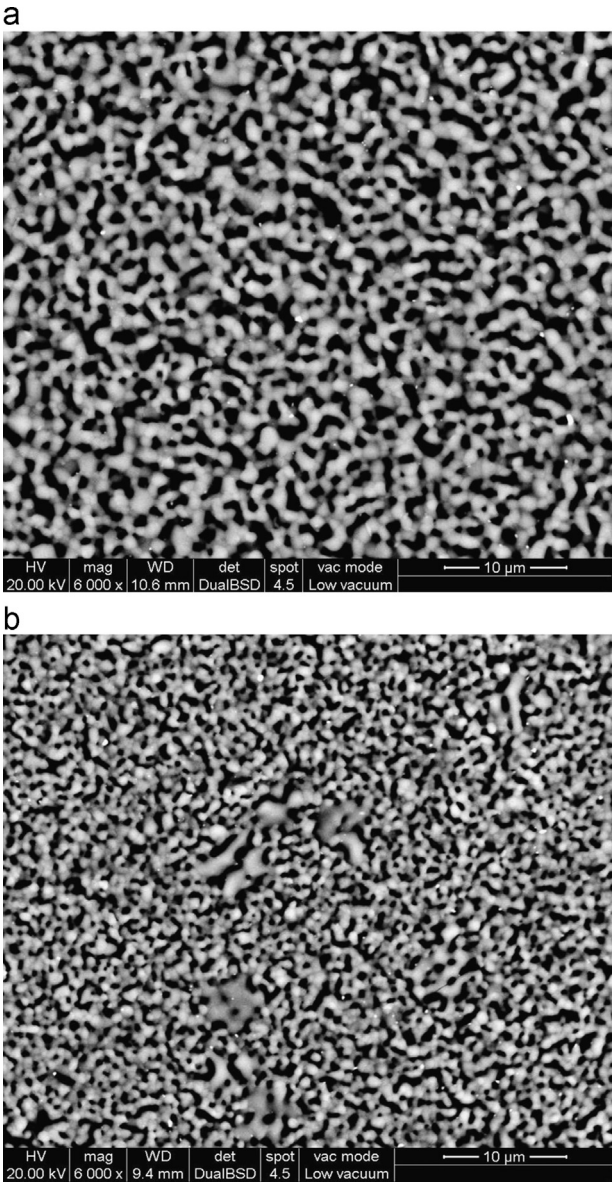

Fig. 5. Microstructure of the FA coating layer after sintering produced using the different dip coating slips: (a) with latex and (b) with PVA.

coalescence during sintering might contribute to the enlargement of the pores in the layer. The onset of the latex coalescence is expected to occur during the drying of the layer when the volume fraction of latex particles approaches 0.6, its maximum solids loading [21]. The latex coalescence resulted in an increase in the particle size of the latex, thereby increasing the pore size left by the latex during burnout. The pores could also coalesce during sintering so that the pore size increased. The greater the pore size, the lower the driving force for sintering and shrinkage; the enlargement of the pores leads to a decreased sintering rate [22]. Therefore, the large pores in the layer reduced the sinterability of FA leading to a greater porosity and pore size in the sintered layer. The greater porosity of the sintered layer (ε_m) increased its thickness, $L_{sintered}$, by increasing β (Eqs. (5)–(7)). Thus, the greater thickness of the sintered layer formed using the slip with latex for immersion times $> > 0$ (Eq. (7)) was attributed to: (1) the flocculated slip which increased the permeability of the wet layer and consequently the casting rate, (2) the higher volume fraction of particles in the wet layer and (3) the more porous layer structure produced by the presence of latex. The liquid entrainment mechanism at the initial stage and slip casting for longer immersion times were both accelerated and the layer shrink during sintering was reduced by using the dip coating slip with latex. On the contrary, the initial film adhered and the casting rate thereafter were both decreased and the layer shrink during sintering was increased when the dip coating slip with PVA was used.

3.2. Biological studies

The osteoblastic cell response to the control substrate and the two FA coating layers was assessed in terms of cell morphology, proliferation and matrix mineralization. No major differences in terms of cell culture morphologies were detectable among the control substrate (Z) and the coating layers produced with PVA (P) and latex (L), at all time points evaluated (Fig. 6). At 3 days of culture, the cells were polygonal in shape, exhibiting long cytoplasmic extensions from which cell–cell contacts were established (Fig. 6a, b and c). Cells with typical morphologies of mitotic division and uni, bi and multidirectional migration could also be observed. After 7 and 12 days of culture, a progressive cell multilayering formation took place on all substrates, showing a large number of mitotic cells and no contact guidance.

Fig. 7 shows the cell proliferation on the control substrate (Z) and on the coating layers produced with PVA (P) and latex (L), at 3, 7 and 12 days of culture. For the control substrate and both coating layers, the number of cells markedly increased with the progression of cultures, confirming the favorable cell proliferation behavior. However, the (L) coating layer supported a reduced cell proliferation values compared with (Z) and (P). It is known that the physical properties of the coating layer such as porosity, roughness and morphology affect cell adhesion, spreading and proliferation [23]. The less porous surface of the (P) coating layer appeared to be favorable for the cell proliferation compared with the more porous surface of the (L) coating layer. However, considering the osteoblast differentiation sequence, the acquisition of a mature, mineralized matrix-producing phenotype depends on the terminal cell cycle arrest [24], indicating that the porous surface of the (L) coating would be better to promote the osteoblast differentiation. Fig. 8 shows the matrix mineralization (Ca content) of cultures grown on the control substrate (Z) and on the (P) and (L) coating layers at 21 days. The cells on the (L) coating layer exhibited a significantly higher mineralization (greater Ca content) compared with (Z) and (P), corroborating the results on cell proliferation. It is generally agreed that micron- and/or nanoporous material surfaces enhance bone matrix production at the material/tissue interface in vitro and in vivo [25].

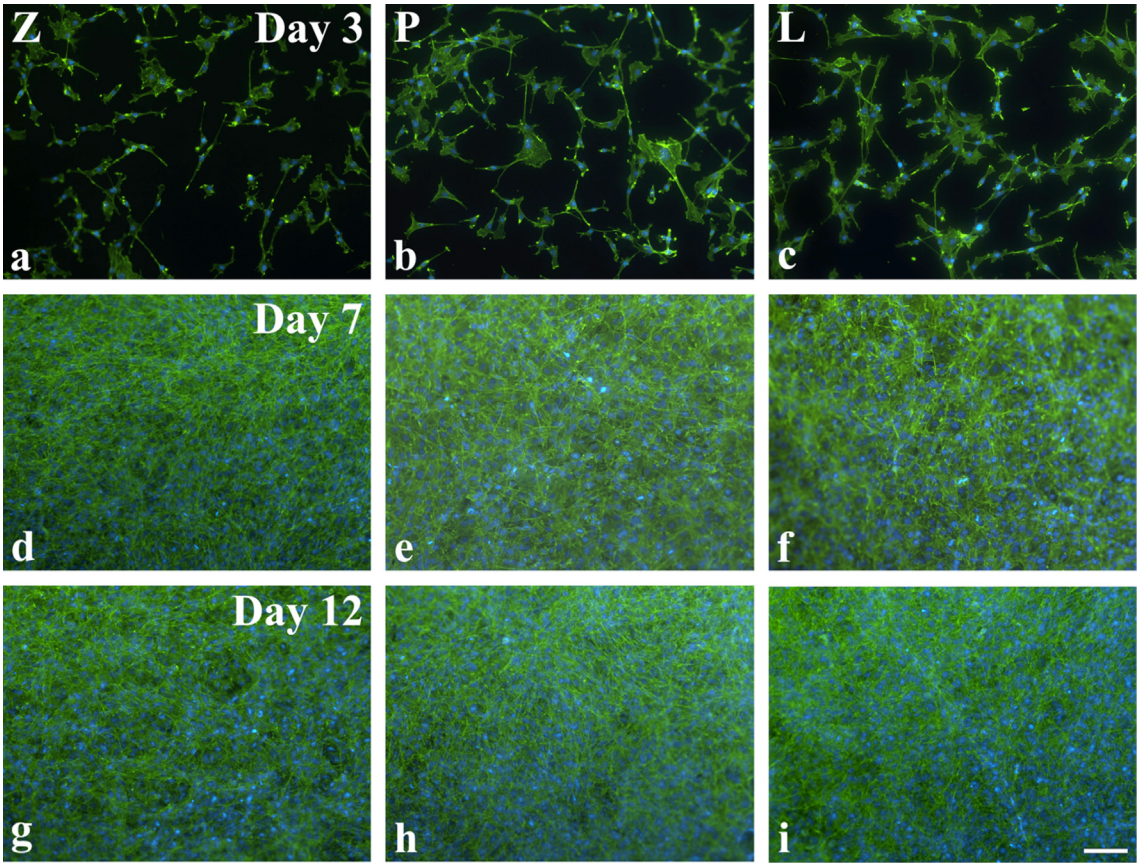

Fig. 6. Epifluorescence of MC3T3-E1 cell cultures grown on the control substrate (Z) and on the coating layers produced with PVA (P) and latex (L), after culturing for 3 (a, b, c), 7 (d, e, f) and 12 (g, h, i) days. Green and blue fluorescence indicate actin cytoskeleton and cell nuclei, respectively. Scale bar = 100 μm. (For interpretation of the references to color in this figure legend, the reader is referred to the web version of this article.)

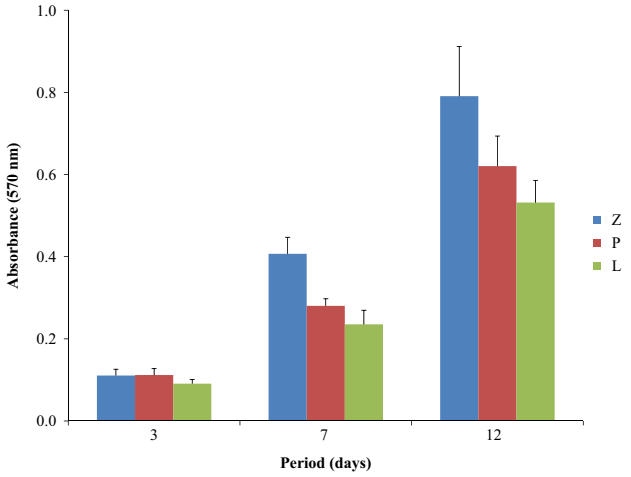

Fig. 7. Cell proliferation of MC3T3-E1 cell cultures grown on the control substrate (Z) and on the coating layers produced with PVA (P) and latex (L), at 3, 7 and 12 days of culture.

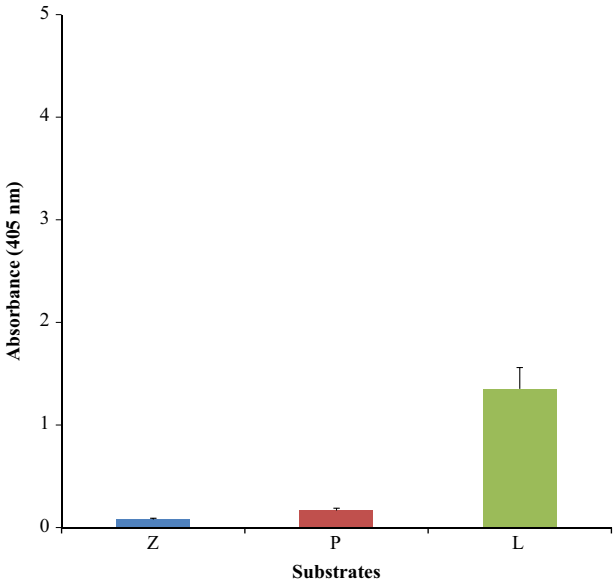

Fig. 8. Matrix mineralization (Ca content) of MC3T3-E1 cell cultures grown on the control substrate (Z) and on the (P) and (L) coating layers, after culturing for 21 days.

4. Conclusions

Fluorapatite layers with different thickness and microstructures on porous Y-PSZ substrates have been fabricated by dipping porous zirconia tapes into aqueous fluorapatite slurries. Porous ZrO_2 tapes were developed using starch and an acrylic latex as fugitive additive and binder, respectively. Two different binders, PVA and latex were used to prepare the fluorapatite dip coating slips.

The formation of a layer on the surface of the tapes was governed by liquid entrainment at the initial stage and slip casting for longer immersion times; both mechanisms were accelerated by using the dip coating slip with latex. A greater initial thickness of the layer adhered was found for the tapes dip coated in the FA slip with latex due to the higher viscosity of the slip and its effect on the liquid entrainment mechanism. For immersion times > 0, the casting rate was observed to be strongly influenced by both the structure of the tape surfaces and the suspension properties.

For both FA slurries, the casting rate at the top surface of the tapes was greater than that at the bottom surface. The migration of the starch and the consolidated latex particles to the top surface during tape casting and drying, respectively, resulted in an increase in porosity of the top surface after sintering relative to that of the bottom surface. Sintered layers with thickness 8–9 times greater on both tape surfaces were found using the dip coating slip with latex. The higher casting rate of the slip with latex was attributed to the greater permeability of the wet layer. Besides, the higher volume fraction of particles in the wet layer and the larger pores in the layer produced by the presence of latex also contributed to increase the thickness of the sintered layer. On the contrary, the film adhered at the initial stage and the casting rate thereafter were both decreased and the layer shrink during sintering was increased when the dip coating slip with PVA was used.

Both FA coating layers supported a reduced cell proliferation compared with the control substrate (Z). The less porous surface of the (P) coating layer appeared to be favorable for the cell proliferation compared with the more porous surface of the (L) coating layer. However, the (L) coating layer enhanced the osteogenic differentiation and consequently the mineralized matrix production by osteoblastic cells.

References

[1] S. Weiner, H.D. Wagner, The material bone: structure–mechanical function relations, Ann. Rev. Mater. Sci. 28 (1998) 271–298.

[2] M. Vallet-Regí, J.M. González-Calbet, Calcium phosphates as substitution of bone tissues, Prog. Solid State Chem. 32 (2004) 1–31.

[3] S.V. Dorozhkin, Nanodimensional and nanocrystalline apatites and other calcium orthophosphates in biomedical engineering, biology and medicine, Materials 2 (2009) 1975–2045.

[4] W. Suchanek, M. Yoshimura, Processing and properties of hydroxyapatite-based biomaterials for use as hard tissue replacement, J. Mater. Res. 13 (1998) 94–117.

[5] L.L. Hench, Bioceramics: from concept to clinic, J. Am. Ceram. Soc. 74 (7) (1991) 1487–1510.

[6] H.-W. Kim, S.-Y. Lee, C.-J. Bae, Y.-J. Noh, H.-E. Kim, H.-M. Kim, J.S. Ko, Porous ZrO_2 bone scaffold coated with hydroxyapatite with fluorapatite intermediate layer, Biomaterials 24 (2003) 3277–3284.

[7] H.-W. Kim, B.-H. Yoon, Y.-H. Koh, H.-E. Kim, Processing and performance of hydroxyapatite/fluorapatite double layer coating on zirconia by the powder slurry method, J. Am. Ceram. Soc. 89 (8) (2006) 2466–2472.

[8] K.-Y. Hung, S.-C. Lo, C.-S. Shih, Y.-C. Yang, H.-P. Feng, Y.-C. Lin, Titanium surface modified by hydroxyapatite coating for dental implants, Surf. Coat. Technol. 231 (2013) 337–345.

[9] W. Weng, J.L. Baptista, Sol–gel derived porous hydroxyapatite coatings, J. Mater. Sci.: Mater. Med. 9 (1998) 159–163.

[10] Y.-H. Jeong, H.-C. Choe, S.-W. Eun, Hydroxyapatite coating on the Ti–35Nb–xZr alloy by electron beam-physical vapor deposition, Thin Solid Films 519 (2011) 7050–7056.

[11] M.P. Albano, L.B. Garrido, K. Plucknett, L. Genova, Processing of porous yttria-stabilized zirconia tapes: influence of starch content and sintering temperature, Ceram. Int. 35 (5) (2009) 1783–1791.

[12] M.P. Albano, L.B. Garrido, Processing of concentrated aqueous fluorapatite suspensions by slip casting, J. Mater. Sci. 46 (15) (2011) 5117–5128.

[13] M.G. Pontin, F.F. Lange, A.J. Sánchez-Herencia, R. Moreno, Effect of unfired tape porosity on surface film formation by dip coating, J. Am. Ceram. Soc. 88 (10) (2005) 2945–2948.

[14] Y. Gu, G. Meng, A model for ceramic membrane formation by dip-coating, J. Eur. Ceram. Soc. 19 (1999) 1961–1966.

[15] H.O. Schwartz Fo, A.B. Novaes Jr., L.M. De Castro, A.L. Rosa, P. Tambasco de Oliveira, In vitro osteogenesis on a microstructured titanium surface with additional submicron-scale topography, Clin. Oral Implants Res. 18 (3) (2007) 333–344.

[16] T. Mosmann, Rapid colorimetric assay for cellular growth and survival: application to proliferation and cytotoxicity assays, J. Immunol. Methods 65 (1983) 55–63.

[17] C.A. Gregory, W.G. Gunn, A. Peister, D.J. Prockop, An alizarin red-based assay of mineralization by adherent cells in culture: comparison with cetylpyridinium chloride extraction, Anal. Biochem. 329 (2004) 77–84.

[18] M.P. Albano, L.B. Garrido, Effect of zirconia tape porosity on fluorapatite film formation by dip coating, Ceram. Int. 39 (1) (2013) 29–37.

[19] M.P. Albano, L.B. Garrido, Processing of concentrated aqueous fluorapatite suspensions by slip casting, J. Mater. Sci. 46 (15) (2011) 5117–5128.

[20] M.P. Albano, L.B. Garrido, Aqueous tape casting of yttria stabilized zirconia, Mater. Sci. Eng. A 420 (2006) 171–178.

[21] J.E. Smay, J.A. Lewis, Structural and property evolution of aqueous-based lead zirconate titanate tape-cast layers, J. Am. Ceram. Soc. 84 (11) (2001) 2495–2500.

[22] D. Kolar, On the role of sintering research in ceramic engineering in sintering processes, Mater. Sci. Res. 13 (1979) 335–367.

[23] K. Anselme, Osteoblast adhesion on biomaterials: review, Biomaterials 21 (2000) 667–681.

[24] G.S. Stein, J.B. Lian, Molecular mechanisms mediating proliferation/differentiation interrelationships during progressive development of the osteoblast phenotype, Endocr. Rev. 14 (4) (1993) 424–442.

[25] R.A. Gittens, R. Olivares-Navarrete, A. Cheng, D.M. Anderson, T. McLachlan, I. Stephan, J. Geis-Gerstorfer, K.H. Sandhage, A. G. Fedorov, F. Rupp, B.D. Boyan, R. Tannenbaum, Z. Schwartz, The roles of titanium surface micro/nanotopography and wettability on the differential response of human osteoblast lineage cells, Acta Biomater. 9 (4) (2013) 6268–6277.